Draft version February 2, 2008
Preprint typeset using LaTeX style emulateapj v. 6/22/04

arXiv:astro-ph/0411752v1 28 Nov 2004

DEFLECTION OF PULSAR SIGNAL REVEALS COMPACT STRUCTURES IN THE GALAXY

Alex S. Hill, Daniel R. Stinebring, Curtis T. Asplund, Daniel E. Berwick,
Wendeline B. Everett & Natalie R. Hinkel
Oberlin College, Department of Physics and Astronomy, Oberlin, OH 44074, USA

Draft version February 2, 2008

ABSTRACT

We have detected a strong deflection of radio waves from the pulsar PSR B0834+06 in scintillation observations. Interference between the undeflected pulsar image and deflected subimages allows single dish interferometry of the interstellar medium with sub-milliarcsecond resolution. We infer the presence of scattering structure(s) similar to those that are thought to cause Extreme Scattering Events in quasar flux monitoring programs: size $\sim$ 0.2 AU (an angular size of 0.1 mas) with an electron overdensity of $\gtrsim 10^3$ compared to the warm ionized medium. The deflectors are nearly stationary in a scattering screen that is thin ($\lesssim 5\%$ of the pulsar-observer distance in extent), is located 70% of the way from the Earth to the pulsar, and has been seen consistently in observations dating back 20 years. The pulsar scans the scattering screen at a velocity of 110 km s^{-1} with a detection radius of 15 mas. Pulsar observations such as these — particularly with a new generation of low-frequency radio telescopes with large collecting areas — hold promise for improving constraints on the poorly understood physical characteristics and space density of the deflecting structures. Such observations may also prove useful in correcting deviations the deflectors produce in high-precision timing of millisecond pulsars.

Subject headings: ISM: structure — pulsars: general — scattering — techniques: spectroscopic — pulsars: individual (PSR B0834+06)

1. INTRODUCTION

The discovery of Extreme Scattering Events (ESEs; Fiedler et al. 1987) in the late 1980s provided evidence for ultracompact ($\lesssim$ 1 AU), ionized objects in the interstellar medium. Despite more than 15 years of observational and interpretive work, the physical conditions, origin, and lifetime of these compact refractors are not well established (Romani et al. 1987; Fiedler et al. 1994; Rickett et al. 1997; Walker & Wardle 1998). Furthermore, their space density and possible contribution to the mass distribution in the Galaxy are poorly known. The basic difficulty has been detecting events in either quasar or pulsar monitoring programs (Walker 2001). In order to substantially affect the flux density of a radio source, the refractor must be nearly aligned with the source. The refractors are typically located at distances of kiloparsecs, so a milliarcsecond alignment is required. Thus, only about a dozen ESEs have been identified, and few of these are easy to model.

The requirement of stringent alignment is relaxed if the intrinsic source size is small enough to exhibit interstellar scintillation, one of the observational consequences of coherent multipath scattering from density inhomogeneities in the medium. Pulsars are the dominant source in this category. Interference between various parts of the pulsar image gives rise to faint but observable periodic fringing patterns in pulsar dynamic spectra (radio flux density as a function of time and observing frequency). These features have a clear representation in the secondary spectrum (the squared modulus of the Fourier transform of the dynamic spectrum) and yield information about the location of the scattering material and the structure of the image (Roberts & Ables 1982; Hewish et al. 1985; Cordes & Wolszczan 1986; Wolszczan & Cordes 1987; Rickett et al. 1997). In particular, periodic fringing in the dynamic fringing gives rise to parabolic *scintillation arcs* (Stinebring et al. 2001; Hill et al. 2003; Cordes et al. 2004; Walker et al. 2004) in the secondary spectrum, which imply that the dominant scattering material is localized in a thin screen along the line of sight.

In this Letter, we present evidence for multiple imaging of the pulsar PSR B0834+06 with greater detail than a similar event reported by Rickett et al. (1997). We detected secondary spectrum features caused by at least five separate ray paths throughout a 26 day observing run. The angular separation between the undeflected pulsar image and each of the four deflected subimages grew linearly at a rate consistent with the velocity of the pulsar. This, combined with multi-frequency data, imply that the multiple imaging is caused by one or several deflecting structures similar to those that cause ESEs and that the structures are stationary in the scattering screen. Such objects, if they trace out underlying neutral material (Walker & Wardle 1998), may contain a significant fraction of the mass of the Galaxy.

2. THIN SCREEN MODEL

We use a model of scintillation arcs developed in Stinebring et al. (2001), Hill et al. (2003), Cordes et al. (2004), and Walker et al. (2004) and summarized here. The essential feature of the model is that a scintillation arc is caused by scattering in a thin screen along the line of sight to the pulsar. Interference between a bright core of the pulsar image and the scatter-broadened halo gives rise to the basic arc, and the details of the power distribution along the arc provide information about the power distribution in the pulsar image. Therefore, our secondary spectra of PSR B0834+06 at 327 MHz provide a partial image of the pulsar with an angular resolution of ~ 0.3 mas and a field of view of ~ 40 mas (see below).

2.1. *Image features and interference patterns*

We define a coordinate system in the plane of the sky with the pulsar at the origin, the $\boldsymbol{\theta}_x$-axis pointing along the effective velocity vector, and $\boldsymbol{\theta}_y \perp \boldsymbol{\theta}_x$. The pulsar effective velocity (Cordes & Rickett 1998),

$$\boldsymbol{V}_{\rm eff} = (1-s)\boldsymbol{V}_{\rm p} + s\boldsymbol{V}_{\rm obs} - \boldsymbol{V}_{\rm s}, \tag{1}$$

is the apparent velocity of the image of the pulsar through the thin scattering screen, where s is the fractional position of the screen from the pulsar ($s = 0$) to the observer ($s = 1$), $\boldsymbol{V}_{\rm p}$ is the transverse velocity of the pulsar, $\boldsymbol{V}_{\rm obs}$ is the transverse velocity of the observer, and $\boldsymbol{V}_{\rm s}$ is the transverse velocity of the screen. Interference between two arbitrary points in the image plane, $\boldsymbol{\theta}_1$ and $\boldsymbol{\theta}_2$, causes fringing in the dynamic spectrum with conjugate time and conjugate frequency of $f_t = -(\boldsymbol{\theta}_2 - \boldsymbol{\theta}_1)\cdot\boldsymbol{V}_{\rm eff}/(s\lambda)$ and $f_\nu = D(1-s)(\boldsymbol{\theta}_2^2 - \boldsymbol{\theta}_1^2)/(2sc)$, where λ is the observing wavelength. The f_ν coordinate is a measure of differential time delay between pairs of rays, and f_t represents the temporal fringe frequency of the interference between the two rays or, alternatively, the differential Doppler shift between them. Interference between the ray at the origin and points along the θ_x-axis produces a parabolic scintillation arc defined by $f_\nu = \eta f_t^2$, where the arc curvature parameter is

$$\eta = \frac{D\lambda^2 s(1-s)}{2cV_{\rm eff}^2}. \tag{2}$$

Interference between the origin and points with non-zero θ_y places power inside the parabola because $f_\nu \propto \theta_x^2 + \theta_y^2$. Interference between a bright spot in the periphery of the image and the the rest of the image produces an inverted parabola or *arclet* with the same $|\eta|$ and a vertex with an f_t coordinate that is related to the θ_x-coordinate[1] of the bright spot by

$$\theta_x = -\left(\frac{s\lambda}{V_{\rm eff}}\right) f_t. \tag{3}$$

Such features are accentuated when the image is elongated along the velocity vector or the bright spot lies near the θ_x-axis, or both.

2.2. *Screen Location*

For pulsars with measured proper motions and measured or estimated distances, we can determine the location of the dominant scattering material from the curvature of the main scintillation arc using equation (2). PSR B0834+06 has an estimated distance (Cordes & Lazio 2003) and a moderately well determined proper motion (Lyne et al. 1982): $D = 0.64 \pm 0.08$ kpc and $\mu = 51 \pm 3$ mas yr^{-1}. We have measurements of scintillation arcs in PSR B0834+06 dating back to 1981 (Stinebring et al. 2005, in preparation). Those data and the observations presented here are consistent with a value of $\eta = 0.47 \pm 0.03$ s^3 at 327 MHz. This results in a value of $s = 0.29 \pm 0.04$ or a screen that is located a distance 0.46 ± 0.08 kpc from the observer. These parameters result in a conversion between f_t and angle on the sky of 50 mHz = 24 mas. Hence, the angular resolution of the secondary spectrum is (2 x 24 mas / 180 pixels) = 0.27 mas per pixel; the useful field of view is about 40 mas.

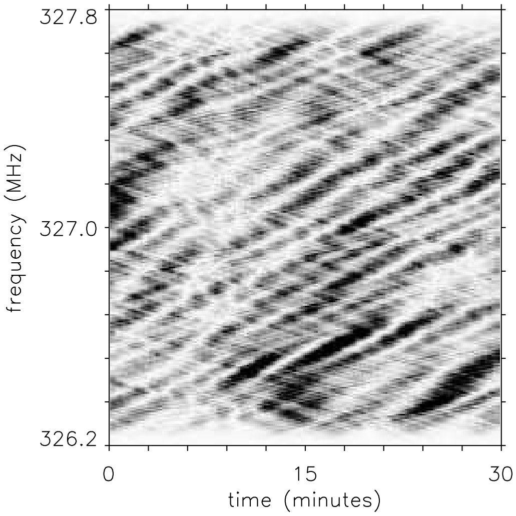

FIG. 1.— The dynamic spectrum of PSR B0834+06 observed on 2003 Dec 31. The flux density as a function of frequency and time is shown using a grayscale that is linear in power, with dark regions indicating high power. The crisscross pattern is due to radio waves reaching the observer from a variety of angles (~ 10 mas away from the pulsar position), as detailed in the text.

3. OBSERVATIONS

To search for evidence of compact refractors using pulsar scintillation, we observed the pulsar PSR B0834+06 at the Arecibo Observatory in 2004 January using the same technique as Hill et al. (2003). An example dynamic spectrum is shown in Figure 1. We obtained dynamic spectra during 30–60 minute integrations using the 327 MHz receiver with spectral resolutions of approximately 1.5 kHz on 11 days over a 26 day period. Typically, we simultaneously took data with center frequencies of 321 and 334 MHz using multiple Wideband Arecibo Pulsar Processor spectrometers. The secondary spectrum in Figure 2 exhibits a scintillation arc as well as numerous arclets. The four isolated arclets, labeled *a*–*d*, shifted upward and to the right along the main parabola during the month. This had never been seen before and is the central observational result of this paper.

4. MOTION OF ARCLETS

We developed an algorithm to locate the position of these arclets in secondary spectra by summing along parabolic regions with vertices incremented along the main parabola. In Figure 3, we plot the fringe frequency of arclet *a* as a function of day number for two closely spaced frequencies. Two models of the refracting structures predict different frequency behavior: if the rays are refracted by smoothly varying electron density variations , the angular position of the rays would scale as is typical for the interstellar medium: $\theta \propto \lambda^2$ (e. g. Scheuer 1968);

---

[1] The minus sign in equation 3 and in the defintion of f_t is present because negative f_t values correspond to deflected rays in front of the moving pulsar; points behind the moving pulsar (past closest encounter to the deflecting structure) produce a positive f_t feature.

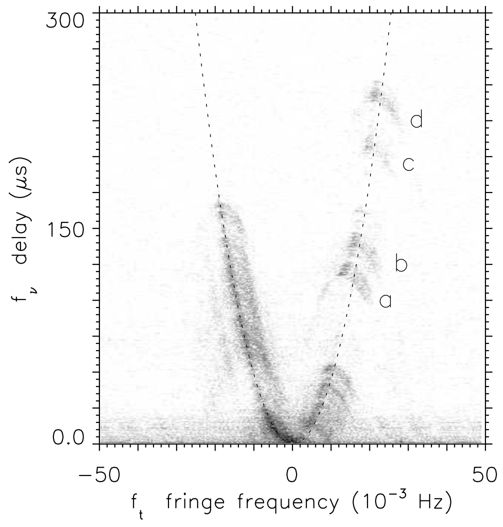

FIG. 2.— The secondary (or delay–fringe-frequency) spectrum corresponding to the dynamic spectrum in Figure 1. The grayscale is logarithmic in power and represents a total range of about 10^5 from the maximum power to the noise level. A primary arc with curvature $\eta = 0.47$ s^3, fitted to the left side of the main parabola, is shown with a dashed line. Numerous inverted parabolas, or *arclets*, are present with vertices near the primary arc. The four isolated arclets (labeled *a*–*d*) each correspond to a distinct enhancement in the pulsar image. The horizontal axis can be converted into a separation angle projected along the direction of pulsar motion using 2 mHz ≈ 1 mas.

then, $f_t \propto \theta\lambda^{-1} \propto \lambda$. Alternatively, if the rays giving rise to the arclets pass through a discrete and dense refracting structure (lens model) (Clegg et al. 1998), they would arrive from nearly the same angle θ at different frequencies; they still deflect as λ^2 within the structure, but only an unmeasurably slight deviation with wavelength occurs because of the small size and high density of the refracting structure. Thus, $f_t \propto \theta\lambda^{-1} \propto \lambda^{-1}$. We performed a least-squares linear fit to the lower frequency data. We then calculated lines with the same slope but vertical offsets scaling as in the lens model and in the smooth variation model. The data in Figure 3 clearly support the lens model, which we assume in the following discussion.

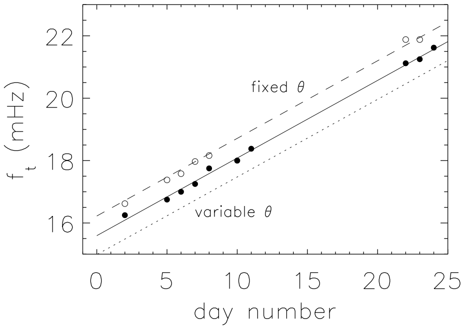

FIG. 3.— The fringe frequency (f_t) coordinate of the vertex of arclet *a* versus day number (day 0 = 2003 Dec 31). Data taken at 321 MHz are plotted with filled circles; 334 MHz data are plotted with open circles, and the uncertainty in position is about the diameter of the symbols. The solid line represents a two parameter fit to the 321 MHz data. The dashed line has the same slope, but with the offset expected if $f_t \propto \lambda^{-1}$, or θ is constant with observing wavelength; the dotted line has the offset expected if $f_t \propto \lambda$, or scattering angle $\theta \propto \lambda^2$. These data indicate that a lens-like structure or structures in the scattering screen causes the arclets.

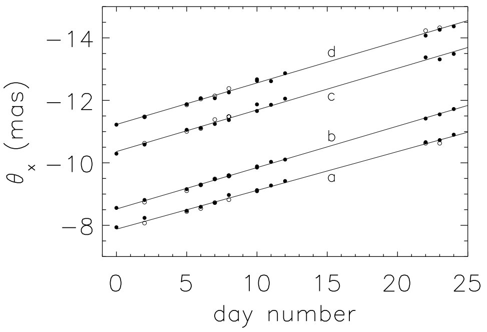

FIG. 4.— The angular position of four arclets over 26 days of observations at two observing frequencies (day 0 = 2003 Dec 31). As in Figure 3, filled circles denote 321 MHz data and open circles indicate 334 MHz data. The uniform, consistent motion of the arclets is primarily due to the motion of the pulsar, indicating that arclets are caused by scattering objects essentially stationary in the screen.

Using measured values of f_t for the vertices of the arclets, we calculated their angular position as a function of time, as shown in Figure 4. Uncertainties in the angular positions were typically 0.2 mas as derived from the scatter about the best fit lines. Arclet *a* moved at a rate of 47 ± 2 mas yr^{-1} and arclets *b*–*d* each moved at 51 ± 2 mas yr^{-1} along the pulsar effective velocity vector. Taking the measured proper motion of the pulsar and accounting for the Earth's motion at this epoch (van de Kamp 1967; Cordes & Rickett 1998) yields an effective pulsar angular velocity of $\mu_{\rm eff} = 50 \pm 3$ mas yr^{-1}. Hence the angular motion of the pulsar, determined from astrometry, and the rate of increase of the pulsar–deflector angle, determined from the data reported here, are consistent within their combined uncertainties. We use this comparison to estimate the motion of the deflector relative to the screen. We find $v_{\rm scr} = (1-s)D(\mu_{\rm arc} - \mu_{\rm eff}) \lesssim 9$ km s^{-1}, implying that the physical objects giving rise to the arclets are essentially stationary in the scattering screen.

5. DISCUSSION

The refracting angle of a plasma lens of size a is $\theta_r \sim \alpha a/D$, where $\alpha \equiv \lambda^2 r_e N_0 D/\pi a^2$ characterizes the strength of the refractive effects, $N_0 = \int n_e ds$ is the maximum electron column density through the lens, and r_e is the classical electron radius (Clegg et al. 1998). If we define an average electron density $\bar{n}_e \equiv N_0/a$, then $\bar{n}_e = (5.4\ {\rm cm}^{-3})\theta_{\rm r}/\lambda^2$, where the angle is measured in mas and the wavelength is expressed in meters. For $\theta_r \approx 15$ mas at 327 MHz, we find $\bar{n}_e \approx 100$ cm^{-3}, which is more than 10^3 times greater than the average electron density in the interstellar medium (Cordes & Lazio 2002).

The thinness of the arclets is remarkable as well and reinforces the interpretation of refraction by lens-like structures embedded in a thin scattering screen. The arclets in Figure 2 have a fractional thickness of $\Delta f_\nu / f_\nu \approx 5\%$.

Since $f_\nu \propto \theta^2$, this implies $a \sim \Delta\theta(1-s)D \approx 0.1$ AU if each arclet is produced by a separate refractor. In this case the mass in each refractor is only $M \sim a^3 \bar{n}_e m_H \approx 10^{-18}\, M_\odot$; here m_H is the mass of a hydrogen atom and we are assuming a fully ionized object.

Instead of four separate deflecting structures, the four arclets may be caused by two or even just one structure. The basic imaging features of a plasma lens become apparent by analyzing a simple model with a Gaussian column density (Clegg et al. 1998). This model predicts caustic surfaces where rays intersect and a defocusing region directly in front of the lens. In the region between the inner caustic and the outer caustic an observer would see a bright undeflected image of the source and two dim, deflected subimages, which would give rise to two arclets as the subimages interfere with the central image. The angular separation between a pair of arclets remains constant, as in these observations, for the arclet pairs *ab* and *cd*, if the refractive strength parameter $\alpha \gg 1$; in this case, $\Delta\theta \approx 2a/(D - sD)$ and $\bar{n}_e = \pi\alpha(1-s)\Delta\theta/(2\lambda^2 r_e) \approx (1.9\ \mathrm{cm}^{-3})\alpha\Delta\theta_{\mathrm{mas}}/\lambda^2_{\mathrm{meter}}$. We can estimate α from the observations because the brightness of the deflected image relative to the central image is $\approx (1+\alpha)^{-1}$. The peak power of the arclets in Figure 2 is about 10^{-3} of the power at the origin in the secondary spectrum, so $\alpha \gtrsim 10^3$. Using this model, our observations yield estimates of $a \approx 0.25$ AU, $\bar{n}_e \sim 2000\ \mathrm{cm}^{-3}$, and $M \approx 4 \times 10^{-16}\, M_\odot$. It should be noted that neither of these models is in pressure balance in the warm ionized phase of the interstellar medium; hence, they would be expected to dissipate quickly unless constrained through some other mechanism (Romani et al. 1987; Rickett et al. 1997; Walker & Wardle 1998).

Walker & Wardle (1998) proposed a model for ESEs in which compact (~ 1 AU), long-lived spheroids of neutral hydrogen are surrounded by a photoionized shell. This results in a double-peaked electron column density profile; each peak may give rise to two enhancements in the image, resulting in the observed four-arclet pattern. In this case, $a \approx \Delta\theta_{ad}(1-s)D/2 \approx 1$ AU, where $\Delta\theta_{ad} = 3.3$ mas is the separation between arclets *a* and *d*. The mass encompassed by the refracting structure is dramatically higher in this model ($M \sim 10^{-3} M_\odot$) because of the unionized, cold, dense core. A Galactic halo population of these clouds, sufficient to account for the poorly constrained ESE rate, would be a major contributor to the total mass of the Galaxy.

Because interference effects are present even when the deflector does not intercept the line of sight, pulsar scintillation observations will improve constraints on the space density of the deflecting structures. The angular offset of the deflector(s) from the θ_x-axis is an important parameter in estimating their space density. Analysis of these data yields θ_y offsets in the range 2 – 6 mas. Our sensitivity to this level of offset, along with the ability to detect deflectors within 10–15 mas on either side of the pulsar, greatly increases the detection probability compared to flux-only observations.

6. CONCLUSIONS

Scintillation observations provide greater detail on the physical properties of these refractors than quasar flux monitoring for two principal reasons. First, the interference between the deflected and undeflected images of the pulsar allows a single dish telescope to act as an interferometer with excellent angular resolution. Second, pulsars scan the scattering screen quickly because of their high transverse velocity. The data presented here demonstrate that dense, compact refractors similar to those that give rise to ESEs can be detected in pulsar scintillation observations. The refracting structures are of interest in their own right, but they also affect high-precision timing of pulsars (Cognard et al. 1993). Since this is one of the most promising methods of detecting a background of primordial gravitational waves, the ability to detect – and potentially correct for – the effects of refracting structures is of practical importance as well.

We currently do not have enough data containing arclets to decide between models or to place realistic limits on the space density of refracting structures. Arclets are not rare, however, particularly at lower frequency ($\lesssim$ 400 MHz) where the effects of scattering and refraction are more pronounced. We have seen arclets, on occasion, in data from pulsars (PSR) B0355+54, B0823+26, B0834+06, B1133+16, B1642–03, B1737+13, and B1919+21. Rickett et al. (1997) identified what is probably a poorly-resolved arclet in B0834+06, and Cordes & Wolszczan (1986) and Wolszczan & Cordes (1987) report similar features in observations of B0919+06 and B1237+25. We are analyzing all of these data further in order to obtain a realistic estimate of the space density of deflectors. It is clear, however, that single-dish scintillation observations with adequate sensitivity at low frequency can be used to track deflectors with milliarcsecond resolution and to estimate their physical properties.

The observations were made at the Arecibo Observatory, which is operated by Cornell University under a cooperative agreement with the National Science Foundation. The research was supported by National Science Foundation grant AST 00-98561.

REFERENCES

Clegg, A. W., Fey, A. L., & Lazio, T. J. W. 1998, ApJ, 496, 253

Cognard, I., Bourgois, G., Lestrade, J. F., Biraud, F., Aubry, D., Darchy, B., & Drouhin, J. P. 1993, Nature, 366, 320

Cordes, J. M. & Lazio, T. J. W. 2002, preprint (astro-ph/0207156)

—. 2003, preprint (astro-ph/0301598)

Cordes, J. M. & Rickett, B. J. 1998, ApJ, 507, 846

Cordes, J. M., Rickett, B. J., Stinebring, D. R., & Coles, W. A. 2004, ApJ, submitted (astro-ph/0407072)

Cordes, J. M. & Wolszczan, A. 1986, ApJ, 307, L27

Fiedler, R., Dennison, B., Johnston, K. J., Waltman, E. B., & Simon, R. S. 1994, ApJ, 430, 581

Fiedler, R. L., Dennison, B., Johnston, K. J., & Hewish, A. 1987, Nature, 326, 675

Hewish, A., Wolszczan, A., & Graham, D. 1985, MNRAS, 213, 167

Hill, A. S., Stinebring, D. R., Barnor, H. A., Berwick, D. E., & Webber, A. B. 2003, ApJ, 599, 457

Lyne, A. G., Anderson, B., & Salter, M. J. 1982, MNRAS, 201, 503

Rickett, B. J., Lyne, A. G., & Gupta, Y. 1997, MNRAS, 287, 739

Roberts, J. A. & Ables, J. G. 1982, MNRAS, 201, 1119

Romani, R., Blandford, R. W., & Cordes, J. M. 1987, Nature, 328, 324

Scheuer, P. A. G. 1968, Nature, 218, 920

Stinebring, D. R., McLaughlin, M. A., Cordes, J. M., Becker, K. M., Espinoza Goodman, J. E., Kramer, M. A., Sheckard, J. L., & Smith, C. T. 2001, ApJ, 549, L97

van de Kamp, P. 1967, Principles of Astrometry (San Francisco: W. H. Freeman and Company)

Walker, M. 2001, Astrophys. & Space Sci., 278, 149

Walker, M. & Wardle, M. 1998, ApJ, 498, L125

Walker, M. A., Melrose, D. B., Stinebring, D. R., & Zhang, C. M. 2004, MNRAS, 354, 43

Wolszczan, A. & Cordes, J. M. 1987, ApJ, 320, L35